JOURNAL OF SOLID STATE CHEMISTRY 110, 274–289 (1994)

Syntheses, Structures, and Characterization of 5-Layer $BaVO_{3-x}$ ($x = 0.2, 0.1, 0.0$)

Guo Liu and J. E. Greedan[1]

Institute for Materials Research, McMaster University, Hamilton, Ontario, Canada L8S 4M1

Received May 18, 1993; in revised form September 3, 1993; accepted September 15, 1993

A 5-layer mixed valence oxide, $BaVO_{2.8}$, has been synthesized by reducing $Ba_2V_2O_7$ in high purity hydrogen gas at 1350°C. $BaVO_{2.9}$ has been obtained by room temperature oxidation of $BaVO_{2.8}$ in air and $BaVO_{3.0}$ obtained by annealing $BaVO_{2.8}$ or $BaVO_{2.9}$ at 200°C in air. The structures of this series of novel compounds have been refined by the Rietveld method using neutron and X-ray diffraction data. Magnetic and electrical properties were examined down to 5 K. All three compounds crystallize in the hexagonal system, space group $P\bar{3}m1$ and $Z = 5$. Lattice parameters (Å) derived from Si-calibrated Guinier X-ray diffraction data are: $BaVO_{2.8}$, $a = 5.7800(2)$, $c = 11.8969(6)$; $BaVO_{2.9}$, $a = 5.7215(5)$, $c = 11.685(2)$; and $BaVO_{3.0}$, $a = 5.6650(3)$, $c = 11.4629(6)$. The $BaVO_{2.8}$ structure consists of face-sharing VO_6^{8-} and VO_6^{9-} octahedra that form $V_3O_{12}^{14-}$ trimers and of VO_4^{4-} tetrahedra that share corners with the trimers. The $BaVO_{2.9}$ and $BaVO_{3.0}$ structures are similar to $BaVO_{2.8}$, except that the VO_4^{4-} tetrahedra in the latter are replaced by VO_6 octahedra in the former compounds. The previously reported 24R $Ba_8V_7O_{22}$ is found to be an intergrowth product of 5H $BaVO_{2.8}$ ($Ba_5V_5O_{14}$) and 9R $Ba_3V_2O_8$. The hydrogen reduction mechanism of $Ba_2V_2O_7$ is examined and the initial formation of $Ba_3V_2O_8$ in the temperature range 650 to 1200°C has been proven by neutron diffraction. The low stability of $BaVO_{2.8}$ is analyzed in terms of stress relief of the face-sharing octahedra and the mobility of the unshared tetrahedron corner oxygens. The electrical conductivity increases dramatically with increasing oxygen content in the $BaVO_{3-x}$ series ($x = 0.2$, 0.1, and 0.0). $BaVO_{2.8}$ and $BaVO_{2.9}$ are semiconductors with room temperature resistivities of about 30 and 0.14 $\Omega \cdot$ cm, respectively. $BaVO_{3.0}$ is metallic with a room temperature resistivity of 0.013 $\Omega \cdot$ cm. The magnetic susceptibility of $BaVO_{2.8}$ shows a broad maximum at about 20 K, indicative of short range order. The susceptibility of $BaVO_{2.9}$ has both temperature-independent and Curie–Weiss type paramagnetic contributions, and $BaVO_{3.0}$ primarily exhibits Pauli paramagnetism.

INTRODUCTION

Our recent investigation of oxides of d^1 V(IV), the one-electron analog of the one-hole d^9 Cu(II), has led to the synthesis of novel oxides containing the rare tetrahedral VO_4^{4-} coordination and exhibiting interesting magnetic properties. For example, the metastable phase of Sr_2VO_4 consists of $V_2O_8^{8-}$ dimers and exhibits dimer-type short-range magnetic correlations (1); Ba_2VO_4 contains isolated VO_4^{4-} but has a one-dimensional magnetic behavior (2). As part of an effort to understand the crystal chemistry and physical properties of VO_4^{4-}-containing oxides, we became interested in the $BaVO_3$ system.

The crystal chemistry of $BaMO_3$-type compounds for many transition metals (M) is characterized by the stacking of hexagonally close-packed BaO_3 layers and the filling of O_6 octahedral holes by the transition metals. Cubic (c) stacking generates corner-sharing MO_6 octahedra, as typified by the perovskite-type (or 3c) $BaTiO_3$ (3), and distorted modifications, while hexagonal (h) stacking leads to face-sharing, as represented by the 2H-type $BaNiO_3$ (4). There exist numerous other polytypes that contain both types of stacking and thus have clusters formed by various modes of corner- and face-sharing of MO_6 octahedra (5). Given the fact that polytypism is known for the two neighbors of vanadium, Ti and Cr, for example, as many as six modifications for $BaCrO_3$ (4H, 6H, 9R, 12R, 14H, and 27R) have been synthesized using high pressure methods (6), one would expect $BaVO_3$ to exhibit polytypism as well, based on the consideration of the relative ionic radius of V(IV) with respect to Ti(IV) and Cr(IV). However, prior to this work very few polytypes were known for the $BaVO_3$ system due to the difficulty of its synthesis. Only a 14-layer and possibly a 12-layer $BaVO_{3-x}$ were synthesized by Chamberland and Danielson (7), again by high pressure methods. Though claims have long been made (8, 9) that a $BaVO_3$ phase containing tetrahedral VO_4^{4-} could be synthesized by hydrogen reduction of $Ba_2V_2O_7$ at about 1200°C, the true identity and structure of the product remained unknown because of the lack of convincing crystallographic evidence.

Torii (10) reported the normal pressure synthesis of 5H $BaCrO_{2.9}$, which was somewhat poorly refined using integrated powder X-ray diffraction intensities. Interestingly, it has a $Ba_5Ta_4O_{15}$-like structure with the additional

[1] To whom correspondence should be addressed.

0022-4596/94 $6.00

Cr occupying the 1*b* site vacant in $Ba_5Ta_4O_{15}$ (11). The 5-layer structure is very rare among existing $BaMO_3$ polytypes for most transition metals except for Nb and Ta, for which only the *M*-deficient forms ($Ba_5M_4O_{15}$ and $Ba_5M_4O_{13}$ (M = Nb, Ta); $Sr_5Ta_4O_{15}$) are known (11). Such a success suggested that ambient pressure synthesis can be an approach to new polytypes for the $BaMO_3$ systems that may not be obtained by high pressure methods. Knowing the problems encountered in the normal pressure synthesis of $BaVO_3$, we carried out detailed studies of the reduction of $Ba_2V_2O_7$ at 1350°C, a temperature substantially higher than previously reported. As a result, we have discovered the first vanadium oxide, $Ba_8V_7O_{22}$, in which V(IV) exists in both tetrahedral and octahedral coordinations and all three common vanadium oxidation states (III, IV, and V) exist in discrete sites (12). In this work, the results for a series of novel 5-layer oxides $BaVO_{3-x}$ (x = 0.2, 0.1, 0.0) are presented.

EXPERIMENTAL

Sample Preparation

Synthesis of $BaVO_{2.8}$. $Ba_2V_2O_7$ was first synthesized by firing an intimate mixture of $2BaCO_3$ (Aesar, 99.9%) and V_2O_5 (Cerac, 99.9%) at 900 to 1000°C for 24 hr in air. Powder specimens of $Ba_2V_2O_7$ were reduced in flowing H_2 gas at 1100°C for 24 hr. About 1.5 g of the black gray product was reground, pelleted, and confined in an open Mo tube (O.D. 1.25 cm) which was secured in an alumina boat and heated in high or ultrahigh purity H_2 gas in a tubular furnace at 1350°C and cooled down rapidly. The reaction time was normally 2 to 4 days, but the completion of the reduction as monitored by Guinier X-ray diffraction was the complete disappearance of the initial product $Ba_8V_7O_{22}$. The pellet surface near both ends of the Mo tube was always partially reoxidized (white), probably during cooling, and the white material was physically removed.

Synthesis of $BaVO_{2.9}$. $BaVO_{2.9}$ was obtained in powder form by exposing pulverized $BaVO_{2.8}$ to air in an open container at room temperature (~20°C) for 4 to 5 months. The sample for the neutron diffraction experiment (about 4 g) was occasionally mixed or reground to assure relatively homogeneous exposure. The same product in pellet form was obtained in 5 to 6 months.

Synthesis of $BaVO_{3.0}$. This phase was obtained by annealing $BaVO_{2.8}$ or $BaVO_{2.9}$ (powder or pellet specimens) at 200°C in air for 24 hr.

Powder X-ray and Neutron Diffraction

Polycrystalline specimens were examined using a Guinier–Hägg camera (IRDAB XDC700) with Cu$K\alpha$1 radiation and a Si standard. The Guinier data were read with a computer-controlled automated LS-20 type line scanner (KEJ Instruments, Täby, Sweden). Step-scanned X-ray powder diffraction data were collected using a Nicolet I2 diffractometer with Cu$K\alpha$ radiation. Neutron diffraction data were collected at the McMaster Nuclear Reactor using 1.3920 Å neutrons obtained by reflection from a Cu [200] monochromator. Details of the neutron data collection and refinement methods have been described previously (13). Data processing was performed on an IBM-compatible 80486 personal computer. Rietveld refinements were effected using the program package DBWS-9006PC, a 1991 release of the PC version of the DBWS3.2S programs by Wiles and Young (14). Powder X-ray data were essential for locating the V atoms which cannot be refined properly with neutron data because of the very small neutron scattering length of vanadium. On the other hand, the neutron data have been used primarily for locating the light oxygen atoms. The vanadium positions from the X-ray data refinement for each compound were used and held fixed in the neutron data refinement, and oxygen positions from the neutron data refinement were used and held fixed in the X-ray refinement. This process was cycled until both refinements converged.

Magnetic Susceptibility and Electrical Resistivity Measurements

Susceptibility data were obtained using a Quantum Design SQUID magnetometer in the temperature range 5 to 300 K using pelleted specimens at an applied magnetic field of 0.2 T. Diamagnetic corrections were applied. Resistivities as a function of temperature were obtained by the van der Pauw method on sintered and annealed pellets. Electrical probes were attached to the specimens with silver paste.

Thermogravimetric Analysis (TGA) and Thermal Tests

The thermogravimetric analysis was performed with a Netzsch STA 409 thermal analyzer in flowing O_2 atmosphere at a heating rate of 5°C/min to 800°C. The final product was phase-pure $Ba_2V_2O_7$ as identified by Guinier X-ray diffraction. The chemical compositions of the three compounds were established by the TGA data and the weight gains at various annealing stages.

RESULTS AND DISCUSSION

Crystal Structures

5H $BaVO_{2.8}$. This material was black, well-crystallized, and phase-pure. TGA analysis established the chemical composition as $BaVO_{2.80(1)}$. Observed Guinier X-ray reflections (27) were indexed completely by TREOR90P, a PC version of the TREOR program (15), to the hexagonal system with a = 5.7800(2) Å, c =

11.8969(6) Å, and remarkably high figures of merit $M(27) = 135$ (16) and $F_{27} = 160$ (17). The absence of any systematic extinction conditions suggested possible space groups $P\bar{3}m1$, $P31m$, $P321$, $P312$, $P\bar{3}m1$, or $P\bar{3}1m$. A literature survey revealed a possible structure model, the 5-layered (5H) $BaCrO_{2.90}$ (10) (space group $P\bar{3}m1$) mentioned above. The observed powder X-ray and neutron patterns of $BaVO_{2.8}$ are in good agreement with those simulated using the program LAZY PULVERIX (18) and the 5H model. Observed Guinier powder reflections are listed in Table 1.

The observed composition is equivalent to the formulation $Ba_5V_5O_{14}$. It was not clear from the existing model whether the oxygens in $Ba_5V_5O_{14}$ are disordered or how

TABLE 1
Observed Guinier Powder X-Ray Diffraction Pattern of $BaVO_{2.80}$

h	k	l	d_{cal}	d_{obs}	I_{obs}
1	0	1	4.6139	4.6111	7
1	0	2	3.8300	3.8283	14
0	1	3	3.1084	3.1082	70
0	0	4	2.9742	2.9736	2
1	1	0	2.8900	2.8903	100
1	0	4	2.5569	2.5566	10
2	0	0	2.5028	2.5036	3
0	2	1	2.4492	2.4487	5
0	0	5	2.3794	2.3793	7
0	2	2	2.3069	2.3068	18
0	1	5	2.1490	2.1489	4
2	0	3	2.1165	2.1167	47
1	1	4	2.0727	2.0727	10
0	2	4	1.9150	1.9151	5
2	1	1	1.8685	1.8684	3
1	0	6	1.8435	1.8434	16
1	1	5	1.8369	1.8372	4
2	1	2	1.8030	1.8027	5
2	0	5	1.7245	1.7248	4
1	2	3	1.7076	1.7076	31
3	0	0	1.6685	1.6686	20
2	1	4	1.5963	1.5961	5
0	2	6	1.5542	1.5540	11
1	2	5	1.4809	1.4810	3
1	1	7	1.4650	1.4650	4
0	3	4	1.4552	1.4552	4
2	2	0	1.4450	1.4450	22
1	0	8	1.4255	1.4255	4
2	1	6	1.3688	1.3687	15
3	1	3	1.3103	1.3104	16
2	0	8	1.2785	1.2781	8
0	1	9	1.2781		
1	1	9	1.2021	1.2020	6
3	1	5	1.1991	1.1989	4
0	4	3	1.1934	1.1934	12
2	1	8	1.1692	1.1689	6
2	0	9	1.1689		

Note. 5H structure, space group $P\bar{3}m1$ (no. 164), $a = 5.7800(2)$ Å, $c = 11.8969(6)$ Å, $V = 344.20(2)$ Å^3, $Z = 5$.

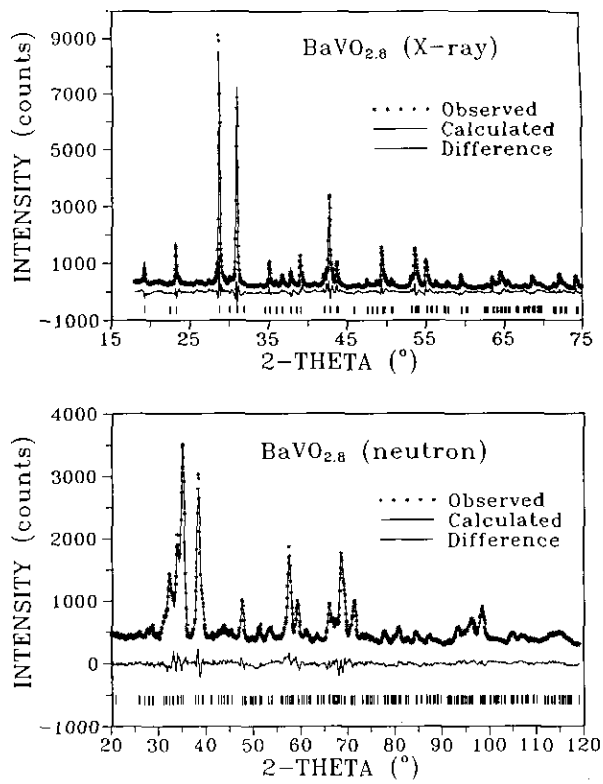

FIG. 1. Observed and calculated X-ray and neutron diffraction patterns of 5H $BaVO_{2.8}$.

the oxygens are arranged if ordered. Initial Rietveld refinement using the neutron data and the $Ba_5Ta_4O_{15}$ oxygen positions (11) indicated the absence of O(1) from the 3*e* site. At this point the known oxygens constituted the composition "$Ba_5V_5O_{12}$," suggesting that two more oxygens were still missing. Interestingly, bond lengths and bond angles of the partially refined structure suggested that V(2) at the 2*d* site was probably tetrahedrally coordinated (3 V(2)–O at 1.82 Å and O(2)–V(2)–O(2)′ at 106°). Hence we proposed that O(1) occupied the 2*d* site, which could explain the observed chemical composition and satisfy the tetrahedral coordination of V(2). Final refinements using both neutron and X-ray data have confirmed this structure for $BaVO_{2.8}$. Observed and calculated neutron and X-ray powder patterns are both shown in Fig. 1. Data collection conditions and refinement details are summarized in Table 2. Atomic parameters are listed in Table 3. Important bond lengths and bond angles are listed in Table 4. The profile fittings are good and structural data are reasonable.

The structure of 5H $BaVO_{2.8}$ is shown in Fig. 2a with emphasis on the VO_4 and VO_6 polyhedra. It is characterized by the vanadium cluster consisting of three face-sharing VO_6 octahedra that form a V_3O_{12} trimer and two corner-sharing VO_4 tetrahedra. A similar cluster has been

TABLE 2
Data Collection Conditions and Refinement Details for $BaVO_{3-x}$ (x = 0.2, 0.1, 0.0)

Compound:	$BaVO_{2.8}$		$BaVO_{2.9}$		$BaVO_{3.0}$	
Diffraction method:	Neutron	X-ray	Neutron	X-ray	Neutron	X-ray
Cell parameters						
a (Å)	5.7755(19)	5.7774(5)	5.692(6)	5.693(6)	5.663(2)	5.6673(8)
c (Å)	11.895(4)	11.893(1)	11.613(12)	11.591(12)	11.459(5)	11.4658(17)
V (Å^3)	343.6(2)	343.77(5)	325.8(6)	325.3(6)	318.2(2)	318.91(7)
2θ Range (°)	20–119	18–74.96	20–105	18–74.96	24–108	18–86.46
Step size (°)	0.10	0.040	0.10	0.040	0.10	0.030
Bragg (R_B)	0.0764	0.0984	0.0539	0.103	0.0938	0.0925
Weighted profile (R_{WP})	0.0651	0.136	0.0659	0.127	0.0771	0.0705
Profile (R_P)	0.0519	0.107	0.0532	0.0990	0.0585	0.0552
Expected (R_E)	0.0421	0.0497	0.0320	0.0530	0.0375	0.0425
Goodness of fit	1.55	2.73	2.06	2.39	2.05	1.66
Profile points (N)	991	1425	851	1425	841	2283
Parameters refined (P)	27	27	26	20	27	24
Independent reflections	309	186	243	174	242	244

Notes.
(a) $R_N = R_B = \Sigma |I_{obs} - I_{cal}|/\Sigma I_{obs}$
$R_{WP} = \{[\Sigma w(Y_{obs} - Y_{cal}/c)^2]/\Sigma w Y^2_{obs}\}^{1/2}$
$R_P = \Sigma |Y_{obs} - Y_{cal}/c|/\Sigma Y_{obs}$
$R_E = [(N - P)/\Sigma w Y^2_{obs}]^{1/2}$
(b) Space group $P\bar{3}m1$ (no. 164), Z = 5.
(c) Wavelengths used: neutron λ = 1.3920 Å; X-ray: Cu $\lambda(K\alpha 1)$ = 1.5406 Å and $\lambda(K\alpha 2)$ = 1.5444 Å.
(d) The no. of independent reflections for X-ray data included those from the $K\alpha 2$ radiation.

observed in $Ba_8V_7O_{22}$ (12). Such a cluster is drawn in Fig. 3a with important bond lengths and bond angles shown. It is worth emphasizing that, like those in $Ba_8V_7O_{22}$, the clusters are not isolated. Instead, they are all connected through corner-sharing and extended in planes perpendicular to the c-axis. Thus, the structure is quasi-two-dimensional.

Using the ionic radii compiled by Shannon (19), the average V–O bond length is expected to be 2.02 Å for a VO_6^{9-}, 1.96 Å for a VO_6^{8-}, and about 1.79 Å for a VO_4^{4-} (based on the ionic radius of 4-coordinated Cr^{4+}). The observed data clearly suggest that V(1) is trivalent ($V(1)O_6^{9-}$: observed 2.03(2) Å), and V(2) and V(3) are tetravalent (observed: 1.78(2) Å for $V(2)O_4^{4-}$ and 1.940(6) Å for $V(3)O_6^{8-}$). As will be discussed further in a later section, these observed data are also in good agreement with those in $Ba_8V_7O_{22}$ (12). $V(1)O_6^{9-}$ is a strongly axially distorted octahedron; $V(3)O_6^{8-}$ is only slightly distorted angu-

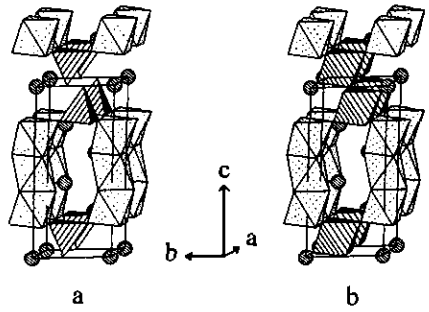

FIG. 2. Crystal structures of 5H $BaVO_{2.8}$ (a) $BaVO_{2.9}$ and $BaVO_{3.0}$, (b) with emphasis on the arrangement of VO_4 and VO_6 polyhedra. Shaded circles are Ba atoms.

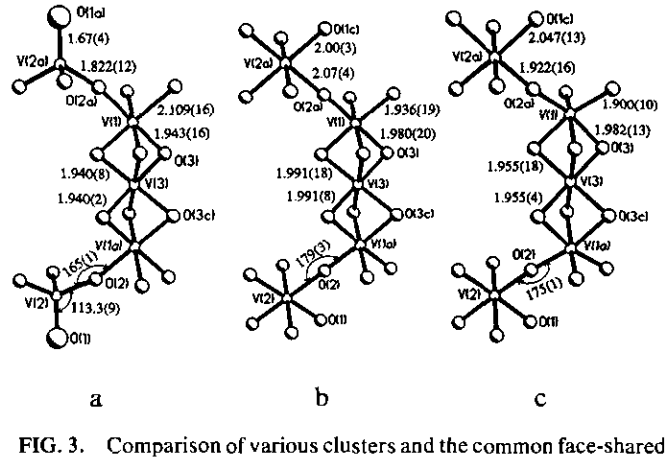

FIG. 3. Comparison of various clusters and the common face-shared V_3O_{12} trimer found in 5H $BaVO_{3-x}$: (a) $V_5O_{18}^{18-}$ ($V(1)_2^{3+}V(2)_2^{4+}V(3)^{4+}O_{18}^{18-}$) in $BaVO_{2.8}$; (b) $V_5O_{21}^{23-}$ in $BaVO_{2.9}$. Note that one of the O(1) oxygens is statistically missing from the $V(2)O_6$ octahedra; (c) $V_5O_{22}^{24-}$ in $BaVO_{3.0}$.

TABLE 3
Atomic Parameters for $BaVO_{3-x}$ (x = 0.2, 0.1, 0.0) from Neutron and X-Ray (in Square Brackets) Profile Refinements

Compound	Atom	Site	x	y	z	B (Å^2)
	Ba(1)	1*a*	0	0	0	0.8(2)
						[2.8(4)]
	Ba(2)	2*d*	$\frac{1}{3}$	$\frac{2}{3}$	0.7624(8)	0.3(2)
					[0.7643(12)]	[1.7(2)]
	Ba(3)	2*d*	$\frac{1}{3}$	$\frac{2}{3}$	0.4176(9)	2.0(3)
$BaVO_{2.8}$					[0.4214(9)]	[2.6(3)]
	V(1)	2*c*	0	0	[0.7006(21)]	[0.9(8)]
	V(2)	2*d*	$\frac{1}{3}$	$\frac{2}{3}$	[0.1297(24)]	[2.3(7)]
	V(3)	1*b*	0	0	$\frac{1}{2}$	[6(1)]
	O(1)	2*d*	$\frac{1}{3}$	$\frac{2}{3}$	−0.0104(19)	9.0(5)
	O(2)	6*i*	0.1662(9)	−0.1662(9)	0.1904(6)	2.1(1)
	O(3)	6*i*	0.1531(7)	−0.1531(7)	0.6001(7)	1.8(1)
	Ba(1)	1*a*	0	0	0	5(1)
						[0.2(3)]
	Ba(2)	2*d*	$\frac{1}{3}$	$\frac{2}{3}$	0.7961(28)	0.7(5)
					[0.7752(16)]	[2.1(4)]
	Ba(3)	2*d*	$\frac{1}{3}$	$\frac{2}{3}$	0.4295(29)	2.0(6)
$BaVO_{2.9}$					[0.4048(15)]	[3.7(7)]
	V(1)	2*c*	0	0	[0.7088(21)]	[3.1(4)]
	V(2)	2*d*	$\frac{1}{3}$	$\frac{2}{3}$	[0.0968(51)]	[3.1(4)]
	V(3)	1*b*	0	0	$\frac{1}{2}$	[3(1)]
	O(1)[a]	3*e*	0.5	0	0	5.5(6)
	O(2)	6*i*	0.1597(19)	−0.1597(19)	0.1957(20)	2.7(3)
	O(3)	6*i*	0.1582(11)	−0.1582(11)	0.6050(19)	0.1(1)
	Ba(1)	1*a*	0	0	0	0.7(9)
						[2.0(2)]
	Ba(2)	2*d*	$\frac{1}{3}$	$\frac{2}{3}$	0.7918(29)	0.6(6)
					[0.7890(6)]	[2.1(2)]
	Ba(3)	2*d*	$\frac{1}{3}$	$\frac{2}{3}$	0.4178(25)	0.9(5)
$BaVO_{3.0}$					[0.4070(7)]	[2.2(2)]
	V(1)	2*c*	0	0	[0.7212(11)]	[3.3(4)]
	V(2)	2*d*	$\frac{1}{3}$	$\frac{2}{3}$	[0.1073(19)]	[2.9(3)]
	V(3)	1*b*	0	0	$\frac{1}{2}$	[1.0(4)]
	O(1)	3*e*	0.5	0	0	0.8(4)
	O(2)	6*i*	0.1704(16)	−0.1704(16)	0.2002(15)	0.6(3)
	O(3)	6*i*	0.1534(16)	−0.1534(16)	0.6088(15)	1.3(3)

[a] Population factor of this site is 0.8333.

larly along the c-axis. $V(2)O_4^{4-}$ has a rather short double-bond-like V–O (V(2)–O(1): 1.67(4) Å); it is a both axially and angularly distorted tetrahedron. The identification of two distinct oxidation states for vanadium, which is consistent with the chemical formulation $Ba_5V_3^{4+}V_2^{3+}O_{14}$, as well as the full occupation of the 2*d* site by O(1), describes a fully ordered structure for $BaVO_{2.8}$.

As will be shown later, the 5H $BaVO_{2.8}$ structure can be derived from the 5H $BaVO_{3.0}$ by changing selected (the corner-sharing only) VO_6^{8-} octahedra into VO_4^{4-} tetrahedra. In this sense, the 5H $BaVO_{2.8}$ structure can be regarded as a brownmillerite analog of the Ba-based "perovskite" (5H $BaVO_{3.0}$). The brownmillerite structures of $CaFeO_{2.5}$ (20, 21) and $SrFeO_{2.5}$ (22) (orthorhombic) consist of perovskite-like layers of FeO_6^{9-} octahedra alternating with layers of FeO_4^{5-} tetrahedra along the long *b*-axis. They can be derived from the perovskite structures of $CaFeO_3$ and $SrFeO_3$ by changing alternate layers of FeO_6^{8-} into FeO_4^{5-} tetrahedra. Of course, there exists a major difference between 5H $BaVO_{2.8}$ and the brownmillerite $CaFeO_{2.5}$ and $SrFeO_{2.5}$ because the tetrahedra in the former structure are formed by vanadium (IV), while those in the latter are formed by the slightly larger sized iron (III).

5H $BaVO_{2.9}$. The black material obtained by room temperature oxidation was somewhat poorly crystallized.

TABLE 4
Selected Bond Lengths (Å) and Bond Angles (°) for $BaVO_{3-x}$ (x = 0.2, 0.1, 0.0)[a] and $Ba_8V_7O_{22}$[b]

Compound	$BaVO_{2.8}$		$Ba_8V_7O_{22}$ (12)		$BaVO_{2.9}$		$BaVO_{3.0}$	
Ba(1)–O(1)	×6	3.3379(9)	×3	3.3412(1)	×6	2.8607(3)	×6	2.8337(4)
Ba(1)–O(2)	×2	2.810(10)	×3	3.340(1)	×2	2.78(3)	×2	2.840(20)
Ba(1)–O(2)′	×2	2.810(8)	×3	2.861(2)	×2	2.78(2)	×2	2.840(18)
Ba(1)–O(2)″	×2	2.810(2)	×3	2.734(2)	×2	2.78(1)	×2	2.840(8)
Average		3.074(6)		3.069(2)		2.82(1)		2.837(8)
Ba(2)–O(1)	×1	2.68(3)	×1	2.657(5)	×3	3.103(16)	×3	2.921(6)
Ba(2)–O(2)	×4	2.939(4)	×6	2.931(1)	×3	2.882(6)	×2	2.837(3)
Ba(2)–O(2)′	×2	2.938(6)			×3	2.882(13)	×4	2.837(9)
Ba(2)–O(3)	×3	2.658(13)	×3	2.685(2)	×3	2.640(24)	×3	2.718(16)
Average		2.83(1)		2.830(2)		2.88(2)		2.828(8)
Ba(3)–O(2)	×3	3.216(12)	×3	3.205(3)	×3	2.99(3)	×3	2.860(17)
Ba(3)–O(3)	×3	2.787(10)	×3	2.784(2)	×3	2.91(2)	×3	2.911(14)
Ba(3)–O(3)′	×5	2.903(4)	×6	3.205(3)	×5	2.864(5)	×5	2.842(5)
Ba(3)–O(3)″	×1	3.460(2)			×1	3.427(5)	×1	2.563(8)
Average		2.999(7)		2.952(2)		2.95(2)		2.84(1)
V(1)–O(2)	×3	2.109(16)	×3	2.050(3)	×3	1.936(19)	×3	1.900(10)
V(1)–O(3)	×3	1.943(16)	×3	1.998(2)	×3	1.982(20)	×3	1.982(13)
Average		2.03(2)		2.024(3)		1.96(2)		1.94(1)
V(2)–O(1)	×1	1.67(4)	×1	1.669(6)	×3	2.00(3)	×3	2.047(13)
V(2)–O(2)	×3	1.822(12)	×3	1.814(2)	×3	2.07(4)	×3	1.922(16)
Average		1.78(2)		1.778(3)		2.04(3)		1.99(2)
V(3)–O(3)	×4	1.940(8)	×4	1.942(2)	×4	1.991(18)	×4	1.955(18)
V(3)–O(3)	×2	1.940(2)	×2	1.942(1)	×2	1.991(8)	×2	1.955(4)
Average		1.940(6)		1.942(1)		1.99(1)		1.96(1)
V(1)···V(3)		2.39(3)		2.482(1)		2.44(2)		2.54(1)
O(2)–V(1)–O(2)′	×3	86.2(8)	×3	83.1(1)	×3	90.1(11)	×3	99.4(7)
O(2)–V(1)–O(3)	×6	93.9(3)	×6	93.2(1)	×6	91.7(6)	×6	88.5(5)
O(2)–V(1)–O(3)	×3	180(1)	×3	175.0(1)	×3	177.5(15)	×3	167.8(9)
O(3)–V(1)–O(3)′	×3	86.1(9)	×3	90.3(1)	×3	86.5(10)	×3	82.3(7)
O(1)–V(2)–O(1)′		—		—	×3	91(2)	×3	87.6(7)
O(1)–V(2)–O(2)′		—		—	×6	88.4(4)	×6	90.0(4)
O(1)–V(2)–O(2)	×3	113.3(9)	×3	113.6(1)	×3	179(3)	×3	177(1)
O(2)–V(2)–O(2)′	×3	105.3(9)	×3	105.0(1)	×3	92(2)	×3	92.2(9)
O(3)–V(3)–O(3)	×3	180	×3	180.0(1)	×3	180	×3	180
O(3)–V(3)–O(3)	×6	86.3(3)	×6	86.0(1)	×6	86.0(5)	×6	83.7(4)
O(3)–V(3)–O(3)	×6	93.7(3)	×6	94.0(1)	×6	94.0(4)	×6	96.3(4)

[a] Lattice and atomic parameters of Ba and V atoms from the X-ray data refinements and atomic parameters of O atoms from neutron data refinements were used except for $BaVO_{2.9}$, where lattice parameters from Guinier data were used.
[b] Appropriate changes of atom labels for $Ba_8V_7O_{22}$ have been made for comparisons.

TGA analysis and the weight gain after oxidation of $BaVO_{2.8}$ gave a chemical composition of $BaVO_{2.90(1)}$. Observed Guinier X-ray reflections (20) were also indexed completely by TREOR90P to the hexagonal system with a = 5.7215(5) Å, c = 11.685(2) Å and reasonably high figures of merit, $M(20)$ = 41 and F_{20} = 25. Observed Guinier X-ray reflections are listed in Table 5. The structure was also refined using the $BaCrO_{2.9}$ (10) and $Ba_5Ta_4O_{15}$ (11) models and by a combination of neutron and X-ray diffraction data. Observed and calculated neutron and X-ray powder patterns are shown in Fig. 4. Data collection conditions and refinement details are also sum-

TABLE 5
Observed Guinier Powder X-Ray Diffraction Pattern of $BaVO_{2.90}$[a]

h	k	l	d_{cal}	d_{obs}	I_{obs}
1	0	1	4.5618	4.5586	4
1	0	2	3.7789	3.7766	18
0	1	3	3.0622	3.0618	73
1	1	0	2.8607	2.860	100
1	0	4	2.5165	2.5181	5
0	2	1	2.4236	2.4237	5
0	0	5	2.3370	2.3395	1
0	2	2	2.2809	2.2809	22
2	0	3	2.0904	2.0909	46
1	1	4	2.0439	2.0441	3
0	2	4	1.8895	1.8893	2
1	0	6	1.8125	1.8132	6
2	1	2	1.7834	1.7839	5
1	2	3	1.6878	1.6880	23
3	0	0	1.6517	1.6518	17
0	2	6	1.5311	1.5301	3
2	2	0	1.4304	1.4303	18
2	1	6	1.3499	1.3498	3
3	1	3	1.2960	1.2958	11
0	4	3	1.1805	1.1807	6

[a] 5H structure, space group $P\bar{3}m1$ (no. 164), a = 5.7215(5) Å, c = 11.685(2) Å, V = 331.27(6) Å^3, Z = 5.

marized in Table 2 and atomic parameters in Table 3. Important bond lengths and bond angles are listed in Table 4. Due to the broadness of reflection peaks caused by the poor crystallinity of $BaVO_{2.9}$, the refinements and atomic positions are not as accurate as those for $BaVO_{2.8}$. One very notable discrepancy is that the lattice parameters derived from neutron and X-ray refinements of $BaVO_{2.9}$ are substantially smaller than those from the Si-calibrated Guinier data. This is believed to be the result of strong correlations of lattice parameters with the unusually large profile parameters (U, V, and W). Thus, the bond lengths and bond angles are evaluated using the unit cell parameters derived from the Guinier data.

Neutron data refinement indicated that O(1) has moved from the 2*d* site in $BaVO_{2.8}$ to the partially occupied 3*e* site (population factor 0.8333), unlike the assumption by Torii (10) that the oxygen deficiency in $BaCrO_{2.9}$ is at the 6*i* O(3) site. The structure is shown in Fig. 2b for comparison with 5H $BaVO_{2.8}$. The two structures are very similar except for the conversion of the $V(2)O_4$ tetrahedron to a $V(2)O_6$ octahedron. The vanadium cluster is shown in Fig. 3b. The average bond length of V(1)–O (1.96(2) Å) seems to suggest a localized tetravalent V(1). V(3)–O (1.99(2) Å) is rather long considering the fact that $V(3)O_6$ shares faces with two octahedra, thus, it is probably trivalent. However, the $V(2)O_6$ octahedron, where half of the six oxygens are statistically missing, has a long average V(2)–O bond length (2.04(3) Å) that can only be possible for a predominantly trivalent vanadium. Taking into account the equivalent formulation of $Ba_5V_4^{4+}V^{3+}O_{14.5}$ for $BaVO_{2.9}$, these results do not really allow a clear-cut assignment of oxidation states to the various vanadium ions. They are probably more or less delocalized, as will be shown later by its magnetic and electrical properties.

It would be interesting to compare the structure of $BaVO_{2.9}$ with the chromium analog $BaCrO_{2.90}$. Unfortunately, the oxygen positions in the latter structure were poorly refined, and thus no meaningful comparisons could be made.

5H $BaVO_{3.0}$. This compound was obtained as a black, pure, and well-crystallized material. Chemical analysis established the composition to be $BaVO_{2.99(1)}$. Reflections (30) were indexed by TREOR90P again to the hexagonal system, a = 5.6650(3) Å, c = 11.4629(6) Å, and V = 318.59(2) Å^3 with high figures of merit, $M(30)$ = 55 and F_{30} = 53. Observed Guinier X-ray data are listed in Table 6. The data clearly indicate that this $BaVO_{3.0}$ phase is isostructural with $BaVO_{2.9}$. Rietveld refinement results have confirmed the 5H structure. Observed and calculated neutron and X-ray powder patterns are shown in Fig. 5. Data collection conditions and refinement details are summarized in Table 2 and atomic parameters in Table

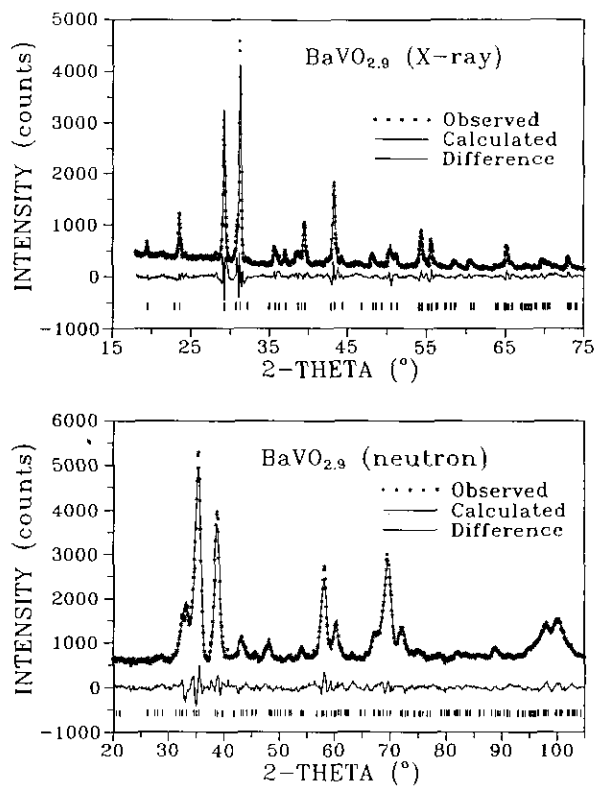

FIG. 4. Observed and calculated X-ray and neutron diffraction patterns of 5H $BaVO_{2.9}$.

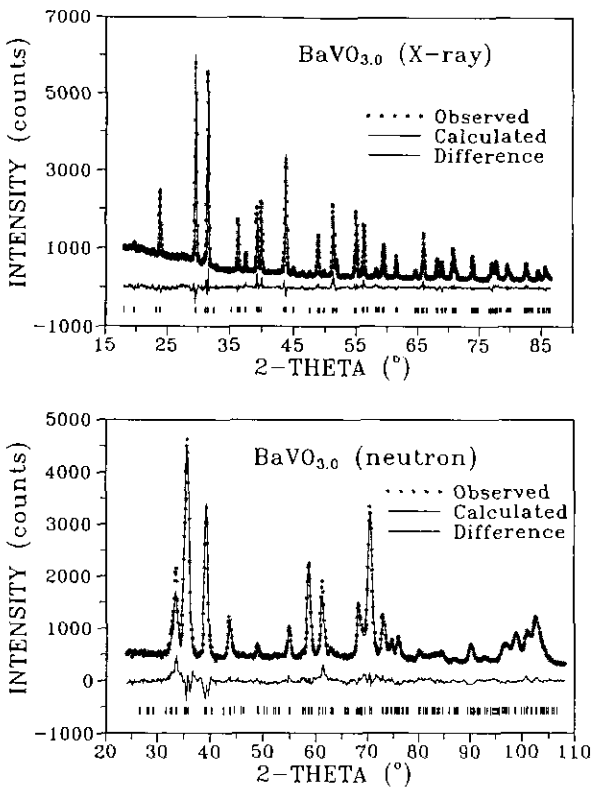

FIG. 5. Observed and calculated X-ray and neutron diffraction patterns of 5H $BaVO_{3.0}$.

3. The structure is essentially the same as that of $BaVO_{2.9}$ (Fig. 2b) except that the 3*e* site is fully occupied by O(1) and that the unit cell dimensions are smaller. Important bond lengths and bond angles are listed in Table 4. Apparently the face-sharing $V(1)O_6^{8-}$ and $V(3)O_6^{8-}$ octahedra are further distorted angularly in $BaVO_{3.0}$ with respect to those in $BaVO_{2.8}$ and $BaVO_{2.9}$, due to significant separation of V(1)···V(3) caused by the increasing repulsion between the vanadium atoms upon oxidation. The corner-sharing $V(2)O_6^{8-}$ octahedron, on the other hand, is strongly distorted axially and has a slightly longer average V–O bond length.

Structural Relationships and the $Ba_2V_2O_7$ Reduction Mechanism

Structural relationship of 24R $Ba_8V_7O_{22}$ with 5H $BaVO_{2.8}$. It has been shown previously that the 24R $Ba_8V_7O_{22}$ structure can be considered as being related to the 12R $BaFeO_{3-x}$ structure (12). However, it was not clear until the 5H $BaVO_{2.8}$ structure became known that the formation of 24R $Ba_8V_7O_{22}$ could be understood. As mentioned briefly in the previous discussion on the $BaVO_{2.8}$ structure, the vanadium cluster found in 5H $Ba_5V_5O_{14}$ is similar to that in $Ba_8V_7O_{22}$. Because $BaVO_{2.8}$ was the final reduction product of $Ba_2V_2O_7$ at 1350°C and $Ba_8V_7O_{22}$ was the initial product under similar experimental conditions, it is likely that the observation of a similar cluster in both compounds signifies an intimate relationship between the two structures. Thus, it is worth examining them closely.

The 5H $BaVO_{2.8}$ and 24R $Ba_8V_7O_{22}$ structures are compared in Fig. 6. The similarity of 5H $BaVO_{2.8}$ (Fig. 6a) with part of the 24R $Ba_8V_7O_{22}$ structure (Fig. 6c) is striking. The similarity is further proven by comparing bond lengths and bond angles of $BaVO_{2.8}$ with those of $Ba_8V_7O_{22}$ related to the $Ba_5V_5O_{14}$-like blocks. As can be seen from Table 4, the values are very close for the most part. The major difference is the slight compression of the $V(1)O_6$ octahedron along the *c*-axis in 5H $BaVO_{2.8}$, resulting in a minor change of the O–V(1)–O bond angles and the shortening

TABLE 6
Observed Guinier Powder X-Ray Diffraction Pattern of $BaVO_{3.0}$[a]

h	k	l	d_{cal}	d_{obs}	I_{obs}
1	0	1	4.5103	4.5041	2
1	0	2	3.7271	3.7261	22
0	1	3	3.0146	3.0141	61
1	1	0	2.8325	2.832	100
1	0	4	2.4745	2.4745	11
0	2	1	2.3987	2.3990	5
0	0	5	2.2926	2.2927	8
0	2	2	2.2552	2.2558	26
0	1	5	2.0770	2.0772	2
2	0	3	2.0642	2.0646	46
1	1	4	2.0145	2.0129	1
0	2	4	1.8635	1.8638	10
2	1	1	1.8305	1.8291	1
1	1	5	1.7820	1.7817	16
2	1	2	1.7643	1.7649	8
2	0	5	1.6749	1.6750	3
1	2	3	1.6682	1.6684	25
1	1	6	1.5839	1.5824	1
2	1	4	1.5568	1.5567	8
0	1	7	1.5533	1.5539	5
0	2	6	1.5073	1.5070	7
1	2	5	1.4417	1.4417	8
2	2	0	1.4162	1.4163	23
1	0	8	1.3754	1.3753	4
0	2	7	1.3620	1.3618	6
2	1	6	1.3306	1.3305	10
1	3	2	1.3239	1.3238	3
3	1	3	1.2818	1.2820	18
2	0	8	1.2373	1.2374	5
1	3	4	1.2292	1.2287	6
1	2	7	1.2274	1.2275	6
2	2	5	1.2049	1.2049	7
4	0	2	1.1994	1.1991	3
0	4	3	1.1678	1.1679	8
0	0	10	1.1463	1.1461	3
2	1	8	1.1338	1.1340	5

[a] 5H structure, space group $P\bar{3}m1$ (no. 164), a = 5.6650(3) Å, c = 11.4629(6) Å, V = 318.59(2) Å^3, Z = 5.

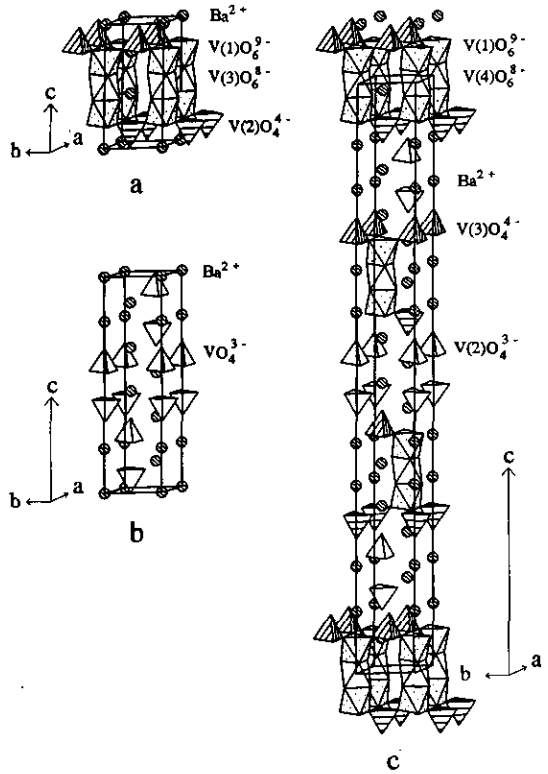

FIG. 6. Structures of (a) 5H $BaVO_{2.8}$, (b) 9R $Ba_3V_2O_8$, and (c) 24R $Ba_8V_7O_{22}$ showing the intergrowth of the 24R from the 5H and 9R structures.

of the V(1)···V(3) distance from 2.482(1) Å in 24R $Ba_8V_7O_{22}$ to 2.39(3) Å in 5H $BaVO_{2.8}$.

Structural relationship of 24R $Ba_8V_7O_{22}$ with (9R) $Ba_3V_2O_8$. According to our previous single crystal X-ray diffraction results, there exist isolated and unreduced VO_4^{3-} groups among other things in the $Ba_8V_7O_{22}$ structure (12). The identification of 5H $Ba_5V_5O_{14}$ blocks in 24R $Ba_8V_7O_{22}$ allows assignment of the remaining blocks as $Ba_3V_2O_8$:

$$Ba_5V_5O_{14} + Ba_3V_2O_8 = Ba_8V_7O_{22}. \quad [1]$$

Interestingly, the formula $Ba_3V_2O_8$ represents a simple but unusually stable V(V) oxide in this system. The structure of $Ba_3V_2O_8$ is shown in Fig. 6b (23). A comparison of Fig. 6b and Fig. 6c suggests that the additional blocks in $Ba_8V_7O_{22}$ are indeed similar to those of $Ba_3V_2O_8$. Important bond lengths and bond angles are compared in Table 7. They are strikingly close as well.

Lattice parameters of the various 5H phases are summarized in Table 8, together with other reported $BaVO_{3-x}$ phases and related compounds. $Ba_3V_2O_8$ also belongs to the rhombohedral system and even has the same space group as $Ba_8V_7O_{22}$. The a-axis, the formula volume, the average layer thickness c/n, and axial ratio $c/(a \cdot n)$ can be considered indicators of the tightness of close-packing and layer-stacking. From Table 8, it is evident that 24R $Ba_8V_7O_{22}$ is an intergrowth of 5H $Ba_5V_5O_{14}$ and (9R) $Ba_3V_2O_8$. These findings provided some of the most important clues and convincing evidence for the proposed reduction mechanism of $Ba_2V_2O_7$ described below.

The $Ba_3V_2O_8$ puzzle. The identification of $Ba_3V_2O_8$ blocks in $Ba_8V_7O_{22}$ gives clues to the solution of the old problem of $Ba_3V_2O_8$ formation during the reduction of $Ba_2V_2O_7$ by H_2 at temperatures below 1200°C. Some early investigations had revealed the formation of a $Ba_3V_2O_8$-like phase even at a temperature as low as about 650°C

TABLE 7
Comparison of Important Bond Lengths (Å) and Bond Angles (°) of 9R $Ba_3V_2O_8$ with Those of its Equivalent Blocks in 24R $Ba_8V_7O_{22}$[a]

Compound	$Ba_8V_7O_{22}$ (12)			$Ba_3V_2O_8$ (23)		
	$Ba(3)O_{10}$			$Ba(2)–O_{10}$		
Ba(3)–O(4)		(×1)	2.628(6)	Ba(2)–O(1)	(×1)	2.61(2)
Ba(3)–O(2)		(×3)	2.820(2)	Ba(2)–O(2)	(×3)	2.80(2)
Ba(3)–O(2)′		(×4)	2.950(2)	Ba(2)–O(2)′	(×4)	2.94(2)
Ba(3)–O(2)″		(×2)	2.950(1)	Ba(2)–O(2)″	(×2)	2.94(2)
Average			2.879(2)	Average		2.87(2)
	$V(2)O_4$			VO_4		
V(2)–O(2)		(×3)	1.720(1)	V–O(2)	(×3)	1.71(3)
V(2)–O(5)		(×1)	1.695(5)	V–O(1)	(×1)	1.70(3)
Average			1.714(2)	Average		1.71(3)
O(2)–V(2)–O(2)′		(×3)	109.5(1)	O(2)–V–O(2)′	(×3)	108.8(4)
O(2)–V(2)–O(5)		(×3)	109.4(1)	O(1)–V–O(2)	(×3)	109.2(3)

[a] Ba(1) of $Ba_3V_2O_8$ is equivalent to Ba(2) of $Ba_8V_7O_{22}$, but it lies in the intergrowth plane with $Ba_5V_5O_{14}$ and thus its coordination environment has changed in $Ba_8V_7O_{22}$.

TABLE 8
Comparison of Selected Layered ABO_3 Type Oxides and $BaVO_{3-x}$ Polytypes

Compound	Structure (n layers)	Space group	a (Å)	c (Å)	Formula volume (Å^3)	Axial ratio $c/(a\cdot n)$	Layer thickness c/n (Å)	Reference
$BaVO_{2.8}$	5H	$P\bar{3}m1$	5.7800(2)	11.8969(6)	68.84	0.4117	2.3784	This work
$BaVO_{2.9}$	5H	$P\bar{3}m1$	5.7215(5)	11.685(2)	66.25	0.4085	2.3370	This work
$BaVO_{3.0}$	5H	$P\bar{3}m1$	5.6650(3)	11.4629(6)	63.72	0.4047	2.2926	This work
$Ba_5Ta_4O_{15}$	5H	$P\bar{3}m1$	5.776(5)	11.82(1)	341.5	0.4093	2.364	[11]
($BaTa_{0.8}O_3$)					68.30			
$BaCrO_{2.90}$	5H	$P\bar{3}m1$	5.732	11.920	67.83	0.4159	2.384	[10]
$Ba_3V_2O_8$	9R	$R\bar{3}m$	5.7845(2)	21.317(1)	205.9	0.4095	2.3686	[24]
($BaV_{0.67}O_{2.67}$)					68.63			
$Ba_8V_7O_{22}$	24R	$R\bar{3}m$	5.7791(4)	57.045(5)	1649.9	0.4113	2.3769	[12]
($BaV_{0.875}O_{2.75}$)					68.75			
$BaVO_3$	14H	$P6_3/mmc$	5.6960(7)	32.122(9)	64.47	0.4028	2.2944	[7]
$BaVO_3$	12R	?	5.726(1)	27.821(6)	65.84	0.4049	2.3184	[7]

(8). The product was initially given the formula $Ba_6V_6O_{19}$ based on the weight loss, and thought to be further reduced to $BaVO_3$ at 1150–1200°C. Except for a few weak reflections, the powder X-ray diffraction patterns of both products were so similar to that of $Ba_3V_2O_8$ that the question of $Ba_3V_2O_8$ formation during hydrogen reduction of $Ba_2V_2O_7$ was raised even at the beginning. Even though numerous chemical and physical methods and different synthesis routes seemed to support the presence of new phases (8, 9), convincing crystallographic evidence was apparently lacking. One piece of evidence from the ^{51}V-NMR experiment suggested that vanadium in these products was tetrahedrally coordinated (8). Unfortunately, it was interpreted as a tetrahedral V^{4+} coordination instead of strengthening the suspicion of $Ba_3V_2O_8$ in which vanadium (V^{5+}) was known to be tetrahedrally coordinated.

Our recent interest in the $BaVO_3$ system and our experiences with $Ba_2V_2O_7$ and $Ba_3V_2O_8$ led us to doubt that a real $BaVO_3$ phase was produced in the early experiments. For example, when relatively large amounts of sample (about 6 g) were used and the weight loss was monitored carefully after hydrogen reduction up to 1200°C with repeated grinding and heating, the product had a nominal composition close to $BaVO_{3.1}$. The X-ray diffraction pattern contained "extra" weak reflections that varied dramatically with reaction temperature and it was consistent with previous observations, but the $Ba_3V_2O_8$-like pattern remained essentially unchanged for samples prepared at temperatures ranging from 650°C to up to 1350°. Besides, the extra reflections from high resolution and accurate Guinier X-ray diffraction data cannot be explained on the basis of previously proposed unit cell parameters (8) or any other multilayer cells. Attempts to index the whole pattern failed. Instead, cell parameters derived from the major reflections, a = 5.7842(4) Å and c = 21.319(2) Å, were essentially identical to those reported for $Ba_3V_2O_8$ (Table 8) (24).

In order to prove crystallographically that the major phase in the initial reduction product is $Ba_3V_2O_8$, a Rietveld analysis has been performed using neutron data collected with the sample obtained by reducing $Ba_2V_2O_7$ at 1200°C for 24 hr. As shown in Fig. 7, this model fits the overall profile well in general (no. 1), but weak "impurity" peaks can be seen. Thus, in the final refinement (no. 2), regions where the second phase contribution is prominent were excluded. Data collection conditions and refinement details are summarized in Table 9. Atomic parameters were compared with those from single crystal X-ray diffraction in Table 10. Both sets of parameters agree remarkably well. Thus, it is reasonable to conclude that $Ba_3V_2O_8$ is indeed the major product when $Ba_2V_2O_7$ is reduced by hydrogen at least below 1200°C.

Unfortunately, we were unable to identify the second phase, which is estimated to be about 5%. The existence of only a few weak reflections makes its identification difficult. The reflections do not belong to any of the reported V_2O_3 or other reduced VO_{2-x} phases. For convenience, this apparently vanadium-rich phase is given the formula Ba_xVO_n ($x < 1$).

Proposed mechanism for the reduction of $Ba_2V_2O_7$ by H_2. Based on the above discussions, the reduction process of $Ba_2V_2O_7$ can now be better understood. The initial reduction causes a decomposition into the unreduced $Ba_3V_2O_8$ and the reduced minor phase Ba_xVO_n:

$$(1.5 - x)Ba_2V_2O_7 \xrightarrow[650<T<1350°C]{H_2} (1 - x)Ba_3V_2O_8 + Ba_xVO_n \quad (x < 1). \qquad [2]$$

TABLE 9
Data Collection Conditions and Refinement Details for $Ba_3V_2O_8$ from Hydrogen Reduction of $Ba_2V_2O_7$ at 1200°C

	Experimental method	
	Powder neutron	Guinier X-ray
Wavelength (Å)	1.3913	1.5406
2θ Range (°)	10–112	
Step size (°)	0.10	
Cell parameters[a]		
a (Å)	5.7714(9)	5.7842(4)
c (Å)	21.248(3)	21.319(2)
V (Å^3)	612.9(1)	617.69(9)
Space group	$R\bar{3}m$	
Z	3	
Bragg (R_B)	0.0424	
Weighted profile (R_{WP})	0.0717	
Profile (R_P)	0.0534	
Expected (R_E)	0.0259	
No. of profile points (N)	1021	
No. of parameters refined	19	
No. of independent reflections	151	

[a] The cell parameters are strongly correlated to the neutron wavelength, which is not reliable enough in this case.

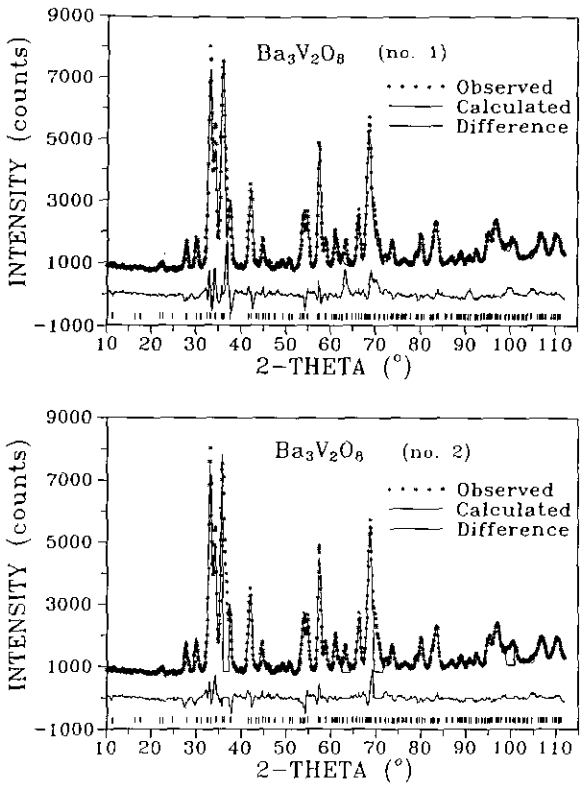

FIG. 7. Observed and calculated neutron diffraction patterns of $Ba_3V_2O_8$ in the product obtained by reducing $Ba_2V_2O_7$ with H_2 at 1200°C. Major impurity peak regions seen in the full-data refinement (no. 1) were excluded in the final refinement (no. 2).

The subsequent reaction is thus essentially the reduction of $Ba_3V_2O_8$ in the presence of Ba_xVO_n. 5H $BaVO_{2.8}$ ($Ba_5V_5O_{14}$) is believed to be the real reduction product:

$$(1 - x)Ba_3V_2O_8 + Ba_xVO_n \xrightarrow[T\geq 1350°C]{H_2} (0.6 - 0.4x)Ba_5V_5O_{14}. \quad [3]$$

$Ba_5V_5O_{14}$ was not observed at the beginning because of its *in situ* intergrowth reaction with $Ba_3V_2O_8$ to form 24R $Ba_8V_7O_{22}$, according to Eq. [1]. The conversion of $Ba_8V_7O_{22}$ into $BaVO_{2.8}$ as the final product is then a simple continuation of the reduction of the $Ba_3V_2O_8$ blocks in the former structure in the presence of remnant Ba_xVO_n.

The above processes can be further described by the layer-stacking models shown in Fig. 8. Using our previously established method (12), 5H $BaVO_{2.8}$ can be described as a 5-layer structure (Fig. 8b) with the (c'chhc) stacking sequence where h and c are hexagonal- and cubic-type BaO_3 layers or pseudolayers, respectively, and c' is a cubic BaO_2 layer. When it is oxidized to 5H $BaVO_{3.0}$, the structure then has the (ccchh) stacking sequence (Fig. 8c). Likewise, the $Ba_3V_2O_8$ structure, which

TABLE 10
Comparison of Atomic Parameters for $Ba_3V_2O_8$ Derived from Powder Neutron Data Refinement with Those from Single Crystal X-Ray Diffraction

		Powder neutron diffraction			Single crystal X-ray diffraction (23)		
Atom	Site	x	z	B (Å^2)	x	z	B (Å^2)
Ba(1)	3a	0	0	1.5(2)	0	0	1.65(5)
Ba(2)	6c	0	0.2053(3)	0.8(1)	0	0.20525(2)	0.96(3)
V(1)	6c	0	0.4076[a]	1.0[a]	0	0.40758(7)	1.42(8)
O(1)	6c	0	0.3280(4)	3.6(1)	0	0.3278(4)	2.5(4)
O(2)	18h	0.1622(5)	0.5642(2)	1.51(7)	0.1610(4)	0.5654(5)	1.0(3)

[a] These parameters were not refined.

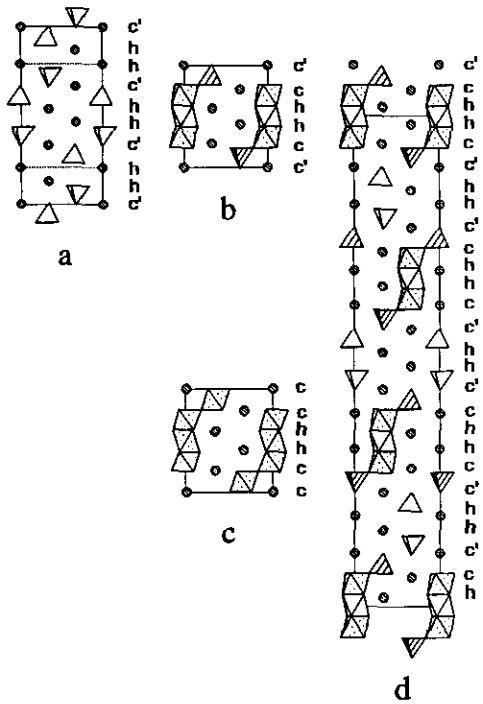

FIG. 8. Layer-stacking sequences of various vanadium oxides: (a) 9R $Ba_3V_2O_8$, (b) 5H $Ba_5V_5O_{14}$ ($BaVO_{2.8}$), (c) 5H $Ba_5V_5O_{15}$ ($BaVO_{3.0}$), and (d) 24R $Ba_8V_7O_{22}$. Shown here are the atoms on the (1 1 0) plane and the VO_4 tetrahedra and VO_6 octahedra of V atoms on (1 1 0). Shaded circles are Ba^{2+} ions; c' is a BaO_2 layer and the others are BaO_3 layers.

has been pointed out previously as having a 9-layer $(chh)_3$ stacking sequence (8), is described as having the $(c'hh)_3$ stacking here (Fig. 8a). Therefore, the intergrowth structure of 24R $Ba_8V_7O_{22}$ can be represented by

$$24R\ (c'hhc'chhc)_3 = 9R\ (c'hh)_3 + 3(5H\ (c'chhc)). \quad [4]$$

The advantage of using the layer-stacking description is that the relationship of the structures of $Ba_5V_5O_{14}$ and $Ba_3V_2O_8$ can be seen more easily. A comparison of Figs. 8a and 8b tends to suggest that the framework of $Ba_5V_5O_{14}$ has a direct root in $Ba_3V_2O_8$, as indicated by the dotted lines. Thus, the conversion of $Ba_3V_2O_8$ and Ba_xVO_n into $Ba_5V_5O_{14}$ under reducing conditions would probably in part involve the insertion of vanadium into the 3*b* site (0 0 ½) in $Ba_3V_2O_8$ and the conversion of c' (BaO_2) to c (BaO_3) layers and some h (BaO_3) to c' (BaO_2) layers at the various planes. Of course, without further evidence a detailed analysis of this process is not justified.

Formation and Stability of the $BaVO_{3-x}$ Phases (x = 0.2, 0.1, 0.0)

The formation of 5H $BaVO_{2.8}$ as the final reduction product of $Ba_2V_2O_7$ is rather slow at 1350°C. Pure specimens can only be prepared in a small quantity (about 1 g) each time in thin pellets (<2 mm), and high purity hydrogen is crucial for the success. The product was contaminated or dominated by the 24R $Ba_8V_7O_{22}$ when the pellet size was too big or too thick, or the sample size was substantially larger than 1 g.

It has been shown that $BaVO_{2.8}$ is unstable toward oxidation even at room temperature (about 20°C). It can be oxidized by atmospheric oxygen to $BaVO_{2.9}$. This process is, however, rather slow at room temperature. The reaction was monitored by the sample weight gain as well as by Guinier X-ray diffraction. As shown in Fig. 9b, the two phases coexisted in the intermediate stages. $BaVO_{2.9}$ obtained in this way was relatively poorly crystallized, as can be seen from its broad X-ray diffraction peaks in Fig. 9c. $BaVO_{2.9}$ can be further oxidized to $BaVO_{3.0}$ at slightly higher temperatures. With mild heating at 100°C in air, both $BaVO_{2.8}$ and $BaVO_{2.9}$ started conversion to $BaVO_{3.0}$, as shown in Fig. 9d. At 200°C, $BaVO_{2.8}$ and $BaVO_{2.9}$ converted to $BaVO_{3.0}$ quantitatively within 24 hr. Due to the oxidation of $BaVO_{2.9}$ toward $BaVO_{3.0}$ even with mild heating, phase-pure $BaVO_{2.9}$ can only be obtained by room-temperature annealing. The coexistence of two or three phases at a certain annealing stage (Fig. 9b and 9d) suggests that there exist three distinct compounds, of which the oxygen contents do not vary significantly from the given stoichiometries. These compounds were eventually oxidized to $Ba_2V_2O_7$ in air at high temperatures (i.e., 800°C).

Thermal tests using pelleted samples in sealed quartz (10^{-4}–10^{-5} Torr) indicated that $BaVO_{3.0}$ started decomposition into poorly crystallized $BaVO_{2.9}$ at 400°C (24 hr),

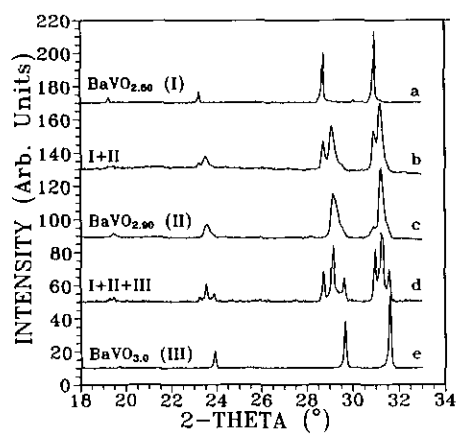

FIG. 9. Low-angle region of the powder X-ray diffraction patterns of the 5H $BaVO_{3-x}$ (x = 0.2, 0.1, 0.0) at various stages. (a) Freshly synthesized $BaVO_{2.8}$; (b) a mixture of $BaVO_{2.8}$ and $BaVO_{2.9}$ obtained after exposing pure $BaVO_{2.8}$ to air for 40 days at room temperature (~20°C); (c) $BaVO_{2.9}$ obtained after 4 months of exposing $BaVO_{2.8}$ to air at room temperature; (d) the formation of $BaVO_{3.0}$ and the coexistence of the three phases after annealing $BaVO_{2.8}$ at 100°C in air for 24 hr; and (e) pure $BaVO_{3.0}$ obtained by annealing $BaVO_{2.8}$ at 200°C in air for 24 hr.

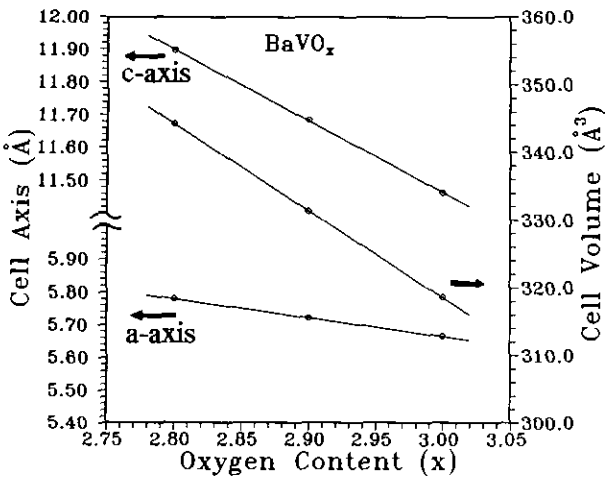

FIG. 10. Change in the *a*- and *c*-axis and unit cell volume as a function of oxygen content (x) in 5H $BaVO_x$ ($2.8 \leq x \leq 3.0$).

and then into $BaVO_{2.8}$ with extended heating or at a slightly higher temperature. At 600°C in sealed quartz, $BaVO_{3.0}$ converted to $Ba_3V_2O_8$ (and possibly another minor reduced phase) almost completely within 4 hr. These results tend to suggest that 5H $BaVO_{2.8}$ is probably a high temperature phase and it is stable only under reducing conditions.

The variation of lattice parameters as a function of oxygen content in $BaVO_x$ (x = 2.8, 2.9, 3.0) is plotted in Fig. 10. Both the *a*- and *c*-axis, and hence the unit cell volume, decrease linearly and drastically with increasing oxygen content. These results suggest that the decrease in the size of vanadium ions due to the increase in their average oxidation state plays a more important role in determining the lattice dimensions than does the increase in the amount of oxygen ions from $BaVO_{2.8}$ to $BaVO_{3.0}$. It can be seen from Table 8 that $BaVO_{2.9}$, especially $BaVO_{3.0}$, have unit cell dimensions close to those of the high-pressure phases, the 14H and possibly the 12R forms of $BaVO_3$ (7).

The cause for the low stability of $BaVO_{2.8}$ toward oxidation is worth a close examination. The first indication comes from the structural evolution from $BaVO_{2.8}$ to $BaVO_{2.9}$. It has been shown that the major change is the conversion of the VO_4 tetrahedra to VO_6 octahedra, namely, the rearrangement of the unshared corner oxygens (O(1)) of $V(2)O_4^{4-}$ tetrahedra in the c′ layers. This result suggests that O(1) in $BaVO_{2.8}$ is highly mobile even at room temperature, which is consistent with the unusually high isotropic temperature factor of O(1) (B = 9.0(5) Å^2, Table 3) compared with those of O(2) (2.1(1) Å^2) and O(3) (1.8(1) Å^2) in the neutron refinement of $BaVO_{2.8}$.

The net chemical change from $Ba_5V_5O_{14}$ to $Ba_5V_5O_{14.5}$ is the oxidation of one V^{3+} into V^{4+}. Knowing that the V^{3+} ions are part of the $V_3O_{12}^{14-}$ trimers in $BaVO_{2.8}$, it is clear that the driving force for the room temperature oxidation of $BaVO_{2.8}$ comes from the trimers and most likely the relief of stress between the face-sharing octahedra of the trimers. As pointed out previously, the V(1)···V(3) distance in $BaVO_{2.8}$ is shorter than the corresponding distance in $Ba_8V_7O_{22}$, indicating that the cluster in the former structure is indeed under greater stress. Thus, the linkage between the VO_4^{4-} tetrahedra and the trimers provides a bridge for the transfer of electronic charges upon oxidation and the minimal structural change from a c′ (BaO_2) to a c (BaO_3) layer, due to the mobility of O(1) in $BaVO_{2.8}$, makes the energy barrier low enough and the geometrical requirement easy to satisfy.

Interestingly, the corresponding tetrahedral corner oxygen, O(4), in the $Ba_8V_7O_{22}$ structure has a rather high isotropic temperature factor as well. The isotropic temperature factor of O(4), 3.2(2) Å^2, is about three to four times larger than those of the corner- or face-shared oxygens (0.79(1) to 1.2(1) Å^2). However, $Ba_8V_7O_{22}$ is stable toward oxidation at least up to 100°C. Apparently the $Ba_5V_5O_{14}$ blocks are stabilized in the intergrowth structure of $Ba_8V_7O_{22}$. This is believed to be due to the fact that half of the oxygens in the c′ layers are part of VO_4^{3-} groups of the stable $Ba_3V_2O_8$ blocks and that the V···V separation in $Ba_8V_7O_{22}$ is longer. This is in contrast to the fact that all oxygens in the c′ layers of $BaVO_{2.8}$ are related to VO_4^{4-} groups.

It is worth noting that the 5H structure is known so far only for Cr and the VB metals (V, Nb, and Ta). The 5H $BaVO_{3-x}$ (x = 0.2, 0.1, 0.0) structures described above represent the first series of well characterized 5H compounds that are not metal deficient. It appears that the larger sizes of Nb(IV, V) and Ta(IV, V) ions and the stability of the trivalent and tetravalent ions of V and Cr play a significant role in the formation of the 5H structures. Further investigations are necessary to better understand the crystal chemistry.

Electrical and Magnetic Properties

The temperature dependencies of the resistivity data of $BaVO_{2.8}$, $BaVO_{2.9}$, and $BaVO_{3.0}$ are shown in Figs. 11, 12, and 13, respectively. There clearly exists an increase in conductivity with increasing oxygen content in this series. $BaVO_{2.8}$ is a semiconductor with a room temperature resistivity of about 30 Ω·cm. In Fig. 11, there are roughly two linear regions with different slopes, corresponding to two activation energies: E_g = 0.52 eV in the temperature range from 290 to 210 K, and E_g = 0.33 eV from 200 to 160 K. Not surprisingly, the electrical properties of $BaVO_{2.8}$ are similar to those of $Ba_8V_7O_{22}$ (12). The activation energies in the lower temperature range are nearly the same in both cases. $BaVO_{2.9}$ is also a semiconductor, but has a much smaller activation energy, E_g =

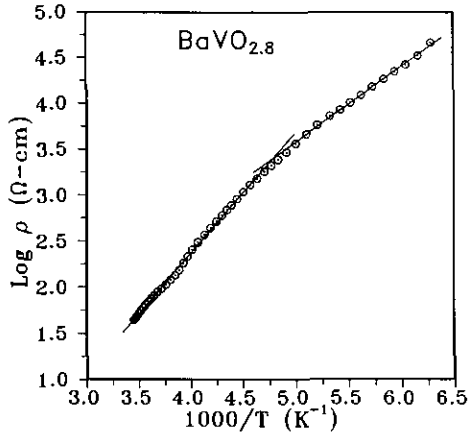

FIG. 11. Thermal variation of the resistivity of 5H $BaVO_{2.8}$. E_g = 0.52 eV from 290 to 210 K, and E_g = 0.33 eV from 200 to 160 K.

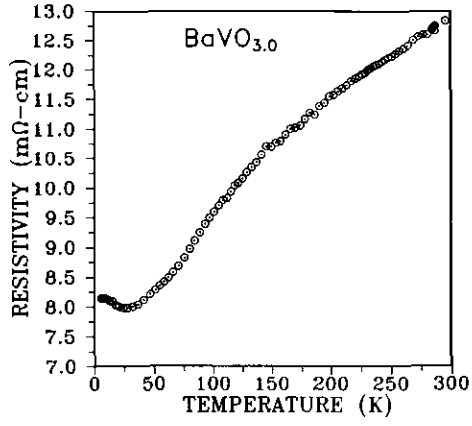

FIG. 13. Thermal variation of the resistivity of 5H $BaVO_{3.0}$.

0.026 eV in the temperature range 295–110 K, and is at least two orders of magnitude more conductive (ρ_{295} = 0.14 Ω · cm) than $BaVO_{2.8}$ at room temperature. $BaVO_{3.0}$, on the other hand, appears to be poorly metallic over a wide temperature range, 300 to about 25 K, with a room temperature resistivity of 0.013 Ω · cm. This high value may be due to the polycrystalline nature of the sample, or it may indicate significant correlation in the 3*d* electrons. Other reports that $BaVO_3$ is semiconducting (9) should be viewed with suspicion as those samples were not well characterized crystallographically. Below 25 K, the resistivity of this $BaVO_{3.0}$ sample increases slightly with decreasing temperature. This may indicate the onset of a metal-to-semiconductor transition, but further work is necessary in order to verify this.

Given that $BaVO_{3.0}$ is metallic over most of the temperature range, it is interesting to note that another metal-to-semiconductor transition occurs upon increasing the V^{3+} and O^{2-} vacancy content. $BaVO_{2.9}$ contains 20% V^{3+} and about 3% oxide vacancies. A parallel situation has been reported for other vanadium(IV) oxides recently. $Sr_3V_2O_7$ is metallic (25), but $La_{1.5}Sr_{1.5}V_2O_7$, containing a much greater V^{3+} concentration, 75%, and nearly zero oxide vacancy concentration, is semiconducting (26). There is an indication that even for V^{3+} levels up to 60%, this system remains metallic (27). Another closely related material is $Sr_4V_3O_{10-\delta}$ (26, 28, 29). This phase is also metallic for $\delta \leq 0.3$, as well as 3% oxide vacancies, but a metal/semiconductor transition occurs for increasing δ (29). Hall effect and resistivity data on polycrystalline samples have been interpreted in terms of a localization mechanism involving a random potential following Mott and Davis (30). It is possible that a similar mechanism can be involved here, but more detailed studies would be necessary to justify this interpretation.

The magnetic susceptibility and inverse susceptibility data of $BaVO_{2.8}$ are plotted in Fig. 14. There exists a broad susceptibility maximum at about 20 K, suggesting

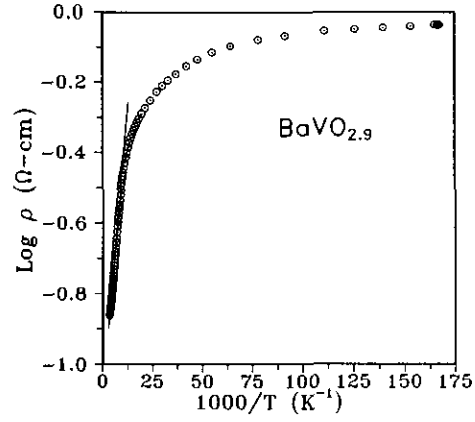

FIG. 12. Thermal variation of the resistivity of 5H $BaVO_{2.9}$. E_g = 0.026 eV from 295 to 110 K.

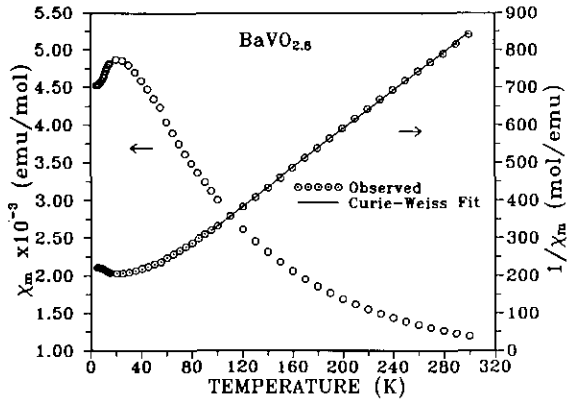

FIG. 14. Temperature dependencies of the magnetic susceptibility and inverse susceptibility of 5H $BaVO_{2.8}$.

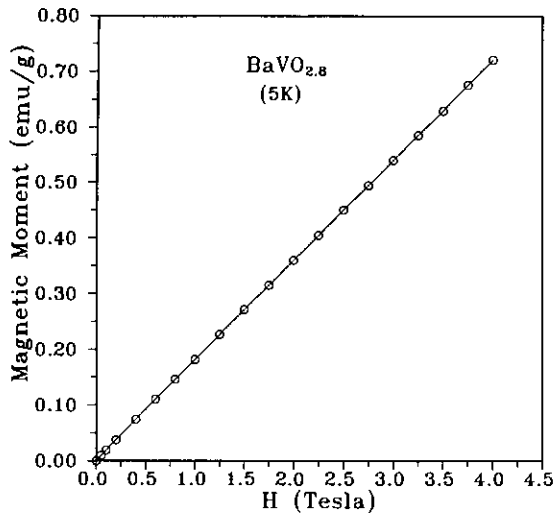

FIG. 15. Field dependency of the magnetic moment of 5H $BaVO_{2.8}$ showing the absence of long-range order.

short-range magnetic correlations. A similar but less prominent behavior has been observed for the powder specimens of $Ba_8V_7O_{22}$ which were probably contaminated by a paramagnetic impurity (12). The data of Fig. 15 indicate an essentially field-independent susceptibility at 5 K.

The high temperature (95–300 K) data of $BaVO_{2.8}$ can be accounted for satisfactorily by the Curie–Weiss law $\chi = C/(T - \theta)$ with correction for a small temperature-independent susceptibility. Least-squares fittings to the observed data gave a Curie constant $C = 0.385(2)$ emu · K/mole, a Weiss constant $\theta = -28.5(7)$ K, and $\chi_{tip} = 1.0(7) \times 10^{-5}$ emu/mole. The value of the Curie constant is very near the value (0.375 emu · K/mole) for an $S = \frac{1}{2}$ system.

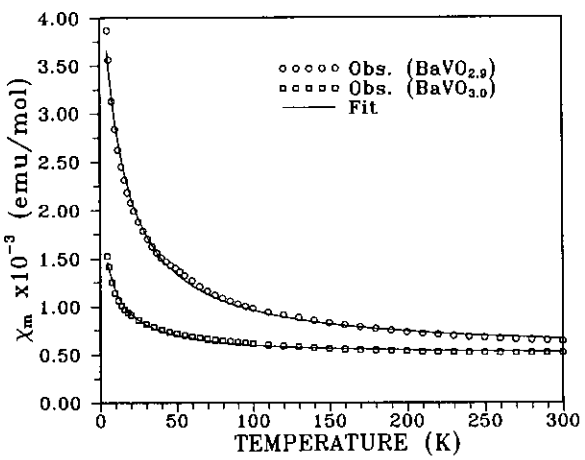

FIG. 16. Temperature dependencies of the magnetic susceptibility of 5H $BaVO_{2.9}$ and $BaVO_{3.0}$. Solid curves are fittings of temperature-independent paramagnetism and Curie–Weiss law.

This is curious as, formally, two of the five vanadium ions per unit cell are vanadium(III), $S = 1$, as in $Ba_5V_3^{4+}V_2^{3+}O_{14}$. Assuming powder-averaged g-factors near 2 and that each vanadium ion is in the paramagnetic state, one calculates an expected Curie constant of 0.625 emu · K/mole. A possible rationalization for the observed value can be made by assuming that the vanadium spins in the face-shared trimeric units are strongly spin-coupled in the temperature range studied. It is further necessary to assume a localization pattern for the ions as V(1) = V(III), V(3) = V(IV). As mentioned in the text, this is supported by bond length considerations. Finally, if the nearest neighbor spins are coupled antiparallel, V(1)($S = 1$)–V(3)($S = -\frac{1}{2}$)–V(1) ($S = 1$), then the ground state for the trimer will be an effective spin $S' = \frac{3}{2}$. If the trimer is not strongly coupled to the spins on the tetrahedral V(2) atoms, this would yield an average spin for the 5-atom cluster $V_5O_{18}^{18-}$ of $S = \frac{1}{2}$. This is now consistent with the observed Curie constant. The broad maximum at low temperatures would then be associated with short-range order either within the cluster or within the five-atom thick layers or blocks which are stacked along the c-axis as shown in Fig. 2a. The connectivity within the blocks is clearly better than that between the blocks, again from Fig. 2a.

The magnetic susceptibility data of $BaVO_{2.9}$ and $BaVO_{3.0}$ are plotted in Fig. 16. Both curves can be explained satisfactorily by a temperature-independent paramagnetism with a Curie–Weiss term. Least-squares fittings gave $\chi_{tip} = 5.02(10) \times 10^{-4}$ emu/mole, $C = 0.0514(1)$ emu · K/mole, and $\theta = -11.3(5)$ K for $BaVO_{2.9}$; and $\chi_{tip} = 4.96(7) \times 10^{-4}$ emu/mole, $C = 0.0116(7)$ emu · K/mole, and $\theta = -6.9(9)$ K for $BaVO_{3.0}$. The two temperature-independent paramagnetic susceptibilities are essentially the same, while the Curie–Weiss contribution is significant for $BaVO_{2.9}$. If one assumes that the Curie–Weiss susceptibility comes from an impurity with spin $S = \frac{1}{2}$, and thus a theoretical Curie constant of $C = 0.375$ emu · K/mole, the impurity level is estimated to be about 14% in $BaVO_{2.9}$ and 3% in $BaVO_{3.0}$. It is thus unlikely in $BaVO_{2.9}$ and 3% in $BaVO_{3.0}$. It is thus unlikely that this Curie–Weiss susceptibility for the $BaVO_{2.9}$ sample originated from an impurity. It is more likely that the Curie constant represents some degree of localization of the vanadium magnetic moments in $BaVO_{2.9}$, as described in the previous section on crystal structures. The predominantly temperature-independent paramagnetism (Pauli paramagnetism) of $BaVO_{3.0}$ is consistent with its observed metallic behavior. The magnitude of this contribution, $4.96(7) \times 10^{-4}$ emu/mole, is large for a one-electron-per-atom system, but is similar in magnitude to that reported for metallic $LaTiO_3$, for which values range from 6.50×10^{-4} to 8.0×10^{-4} emu/mole (31, 32). This is consistent with a highly correlated picture for the d-electrons in $BaVO_{3.0}$.

ACKNOWLEDGMENTS

The financial support of the Natural Science and Engineering Research Council of Canada and the Ontario Centre for Materials Research is acknowledged gratefully. We thank Professor C. V. Stager for use of the magnetometer and Mr. F. Gibbs for obtaining the TGA data.

REFERENCES

1. W. Gong, J. E. Greedan, G. Liu, and M. Bjorgvinsson, *J. Solid State Chem.* **95,** 213 (1991).
2. G. Liu and J. E. Greedan, *J. Solid State Chem.* **103,** 228 (1993).
3. H. D. Megaw, *Nature* **155,** 484 (1945).
4. J. J. Lander, *Acta Crystallogr.* **4,** 148 (1951).
5. J. B. Goodenough and J. M. Longo, *in* "Landolt-Börnstein" (K.-H. Hellwege and A. M. Hellwege, Eds.) Neue Serie III, Vol. 4a, pp. 126–314. Springer-Verlag, Berlin/Heidelberg/New York, 1970.
6. B. L. Chamberland, *Inorg. Chem.* **8,** 286 (1969).
7. B. L. Chamberland and P. S. Danielson, *J. Solid State Chem.* **3,** 243 (1971).
8. A. Feltz and S. Schmalfuss, *Z. Anorg. Allg. Chem.* **417,** 130 (1975).
9. T. Palanisamy, J. Gopalakrishnan, and M. V. C. Sastri, *Z. Anorg. Allg. Chem.* **415,** 275 (1975).
10. Y. Torii, *Chem. Lett.* 557 (1975).
11. (a) F. Galasso and L. Katz, *Acta Crystallogr.* **14,** 647 (1961); (b) J. Shannon and L. Katz, *Acta Crystallogr. Sect. B* **26,** 102 (1970).
12. G. Liu and J. E. Greedan, *J. Solid State Chem.* **108,** 371 (1994).
13. J. N. Reimers, J. E. Greedan, and M. Sato, *J. Solid State Chem.* **72,** 390 (1988).
14. D. B. Wiles and R. A. Young, *J. Appl. Crystallogr.* **14,** 149 (1981).
15. P. E. Werner, L. Eriksson, and M. Westdahl, *J. Appl. Crystallogr.* **18,** 367 (1985).
16. P. M. de Wolff, *J. Appl. Crystallogr.* **1,** 108 (1968).
17. G. S. Smith and R. L. Snyder, *J. Appl. Crystallogr.* **12,** 60 (1979).
18. K. Yvon, W. Jeitschko, and E. Parthé, *J. Appl. Crystallogr.* **10,** 73 (1977).
19. R. D. Shannon, *Acta Crystallogr. Sect. A* **32,** 751 (1976).
20. E. F. Bertaut, P. Blum, and A. Sagnières, *Acta Crystallogr.* **12,** 149 (1959).
21. A. A. Colville, *Acta Crystallogr. Sect. B* **26,** 1469 (1970).
22. M. Harder and Hk. Müller-Buschbaum, *Z. Anorg. Allg. Chem.* **464,** 169 (1980).
23. P. Süsse and M. Buerger, *Z. Kristallogr.* **131,** 161 (1970).
24. Powder Diffraction File card 29-211. JCPDS: International Centre for Diffraction Data, 1601 Park Lane, Swarthmore, PA 19081.
25. A. Nozaki, H. Yoshikawa, T. Wada, H. Yamauchi, and S. Tonaka, *Phys. Rev. B* **43,** 181 (1991).
26. W. Gong, J. S. Xue, and J. E. Greedan, *J. Solid State Chem.* **91,** 180 (1991).
27. D. Spuria and J. E. Greedan, unpublished.
28. M. Itoh, M. Shikano, R. Liang, H. Kawaji, and T. Nakamura, *J. Solid State Chem.* **88,** 597 (1990).
29. N. Ohashi, Y. Teramoto, H. Ikawa, O. Fukunaga, and J. Tanaka, *J. Solid State Chem.* **97,** 434 (1992).
30. N. F. Mott and E. A. Davis, "Electronic Properties in Non-crystalline Materials," 2nd ed. Oxford Univ. Press, Oxford, 1979.
31. D. A. MacLean and J. E. Greedan, *Inorg. Chem.* **20,** 1025 (1981).
32. J. E. Sunstrom IV, S. M. Kauslarich, and P. Klavins, *Chem. Mater.* **4,** 346 (1992).